Int j simul model 17 (2018) 3, 521-533
ISSN 1726-4529 Original scientific paper

MODELLING OF STRAIGHT BEVEL GEAR TRANSMISSION AND SIMULATION OF ITS MESHING PERFORMANCE

Zeng, Q. L.; Wang, K. & Wan, L. R.
College of Mechanical and Electronic Engineering, Shandong University of Science and Technology, Qingdao 266590, China
E-Mail: qlzeng@sdust.edu.cn

Abstract
This paper aims to accurately simulate straight bevel gear transmission, and analyse its exact meshing performance. To this end, the equations for tooth surface, tooth root surface and tooth root transition surface of straight bevel gear were derived based on the gear planning principle. Then, the parametric finite-element modelling of straight bevel gear transmission was realized in ANSYS using surface interpolation technique, and the gear pair meshing was simulated by transient analysis. The tooth surface contact stress and the bending stress were obtained throughout the meshing process. Later, the proposed model was contrasted with three traditional models to verify its feasibility. The results show that the modelling accuracy directly bears on the gear strength, and both the contact stress and the bending stress of the gear varied with the meshing position. The proposed method eliminates the huge errors of the traditional equivalent gear design, and pioneers in the analysis of the meshing features of gear pair. Suffice it to say that this research lays the basis for the accurate design and optimization of straight bevel gear transmission.
(Received, processed and accepted by the Chinese Representative Office.)

Key Words: Straight Bevel Gear, Gear Planning, Tooth Surface Equation, Parametric Modelling, Transient Meshing Analysis

1. INTRODUCTION

The accurate calculation of gear strength is the keystone and difficulty in the field of mechanical design. It is essential to the structural design and optimization of transmission mechanism. Under low-speed and light-load conditions, the straight bevel gear is suitable for transmitting motion and power between two intersecting axes. In the traditional empirical method, the strength of straight bevel gear is calculated by using equivalent spur gear at its midpoint of tooth. However, the calculation has a huge error because of the sharp differences between spur gear and straight bevel gear in tooth profile and meshing conditions.

At present, there are few methods to capture the accurate strength of straight bevel gear. Most of the existing approaches are based on experience. For instance, Bahrami et al. [1] approximated the tooth surface of spur gear by straightening that of straight bevel gear along the tooth width, and computed the Hertzian contact stress of whole tooth surface following the traditional empirical method. However, the accuracy of the calculated results is insufficient. Zolfaghari et al. [2] applied genetic algorithm to optimize the design of straight bevel gear, but the strength calculation was still based on empirical formula. Even worse, the calculation is far from accurate due to the introduction of numerous empirical values.

Recently, the finite-element method (FEM) has emerged as an accurate method to simulate gear loading. There are drawbacks, of course, with the FEM. First, the tooth root transition curve of traditional gear model is replaced by chamfer arc, dragging down the analysis accuracy. Second, the dynamic loading and nonlinear stress change in the meshing process is neglected in the static analysis. Despite the FEM-based accuracy enhancement, most scholars have only tackled the contact strength of tooth surface. Only a few explored the calculation of tooth root bending stress, and replaced the root transition curve with the chamfer arc. Zhang et al. [3] created a straight bevel gear model in SolidWorks, discussed the

contact stress, and gave the spherical involute equation. Nevertheless, the modelling principle of tooth root transition curves was not mentioned. For contact stress analysis, Lou et al. [4] built a 3D model for an axially modified straight bevel gear in ANSYS, failing to provide the tooth surface equation for gear modelling. What is more, the 3D model fails to consider the tooth root transition surface. Zhang et al. [5] probed into the influencing factors of root fatigue failure of micro straight bevel gear, and set up a 3D model for straight bevel gear in ANSYS. The problem is that the tooth root transition curve deviates from the actual shape. To solve the problem, much research has been done on the modelling based on machining principles. Nonetheless, most of the relevant methods did not give a clear indication of the shape of root transition surface. Ozel et al. [6] deduced the tooth surface equation of straight bevel gear by the principle of face milling, yet the computing error was high because the tooth root transition curve was replaced with chamfer arc of the same radius as fillet cutter. Li et al. [7] derived a similar equation based on the principle of double disc milling, failing to provide a clear cutter equation or derived results. Moreover, their research stops at comparing the match degree between processed and theoretical involutes. Following the same principle, Shih and Shieh [8] also obtained the tooth surface equation, and built the corresponding model on modelling software. However, the model may damage tooth root and only applies to special machines. Fuentes et al. [9] worked out the approximate tooth surface equation of straight bevel gear, according to the meshing principle between hypothetical crown gear and bevel gear. Unfortunately, the root transition surface was not deduced and the bevel gear modelling was not fully resolved. Inspired by the principle of hobbing, Cui et al. [10] approximated the machining of straight bevel gear, and created a single gear model for stress analysis. The model deviates significantly from the actual gear structure, owing to the inconsistency between the hobbing principle and the actual machining principle of the straight bevel gear. In general, there is little report on the accurate simulation of the dynamic meshing of straight bevel gear pair. Most of the available resources belong to static analysis. Nalluveeyyil and Muthuveerappan [11] investigated the tooth root bending stress of straight bevel gear with structural parameters at various work conditions. During the simulation, the load was simplified unrealistically as the surface load of a single gear tooth, resulting in a huge analysis error. Based on spherical involute equation, Deng et al. [12] created a 3D model of straight bevel gear in Pro/Engineer, and studied tooth surface contact stress and tooth root bending stress at different meshing angles using ANSYS. Nevertheless, the static analysis of each specified position ignores the impact of dynamic stress variation in the meshing process.

To make up for the defects in the above literature, this paper explores the gear planning principle based on hypothetical plane gear and examines the meshing process of straight bevel gear. Then, a 3D assembly model of straight bevel gear was created based on the accurate tooth surface equations, and a transient meshing analysis was performed in ANSYS. The research findings have a positive impact on the optimization of gear structure design, including the analysis accuracy and design economy.

The remainder of this paper is organized as follows: Section 2 introduces the gear planning principle and derives the meshing equation of straight bevel gear; Section 3 provides the cutting surface equations of cutter; Section 4 deduces the equations for tooth surface, tooth root surface and tooth root transition surface of straight bevel gear based on the principle of gear planning; Section 5 elaborates on the parametric modelling method and performs the simulation analysis in ANSYS; Section 6 presents the simulation example and comparative analysis; Section 7 wraps up this research with some meaningful conclusions.

2. PLANNING PRINCIPLE OF STRAIGHT BEVEL GEAR

2.1 Planning principle based on hypothetical plane gear

During the cutting of straight bevel gear, the tooth profile is generated by the meshing movement, including the rotation of cutter about cradle axis and the rotation of blank about its own axis. Meanwhile, the cutter moves reciprocally along the tooth width, forming the tooth surface. To depict the machining process, three coordinate systems were set up according to the above processing principle. As shown in Fig. 1, $\sigma = \{O; \mathbf{i}, \mathbf{j}, \mathbf{k}\}$ is the fixed coordinate system, where the origin O lies at the thickness midpoint of big-end tooth of straight bevel gear, axis **i** is placed horizontally over O, axis **k** points outward along the reference cone bus of straight bevel gear, and axis **j** is determined by the right-hand rule. $\sigma^{(1)} = \{O_1; \mathbf{i}_1, \mathbf{j}_1, \mathbf{k}_1\}$ is the cutter coordinate system tightly fixed to the cutter. In the initial position, the cutter coordinate system coincides with the fixed coordinate system. $\sigma^{(2)}=\{O_2; \mathbf{i}_2, \mathbf{j}_2, \mathbf{k}_2\}$ is the gear coordinate system that always rotates with the gear. Origin O_2 is the intersection of axis I and axis **j**. The distance from O_2 to O is $R\tan\delta$. In the initial position, axis $\mathbf{j}_2$ coincides with axis **j**, and axes $\mathbf{i}_2$ and $\mathbf{k}_2$ are parallel to axes **i** and **k**, respectively. In the cutting process, the blank rotates around axis I at angular velocity $\boldsymbol{\omega}^{(u)}$. Then, the angular velocity around axis $\mathbf{k}_2$ can be expressed as $\boldsymbol{\omega}^{(2)} = \boldsymbol{\omega}^{(u)}\cos\delta$. The tool rotates around axis II at angular velocity $\boldsymbol{\omega}^{(1)}$ while panning along the OA direction at velocity $\mathbf{V}_{01}$. At time t of the cutting process, the distance between O and O_1 is L_1, and the angular value of the gear coordinate system relative to the initial position is φ_2. The vector expressions of the two variables are $\mathbf{L}_1 = \mathbf{V}_{01}\,t$ and $\varphi_2 = \boldsymbol{\omega}^{(2)}\,t$.

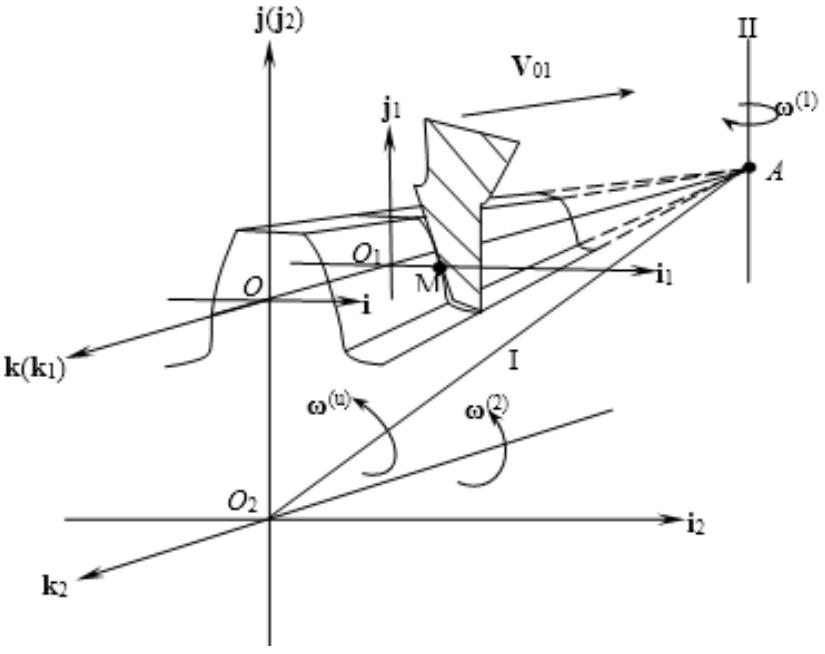

Figure 1: Relative position and coordinate system of cutter and straight bevel gear.

If the contact point between the cutter and the blank tooth surface is denoted as M, then the radial vector of point M in $\sigma^{(1)}$ is $\mathbf{r}^{(1)}$, and the radial vector in $\sigma^{(2)}$ is $\mathbf{r}^{(2)}$. In the course of cutting, $\boldsymbol{\omega}^{(1)}$ can be expressed by $\boldsymbol{\omega}^{(2)}$ as $\boldsymbol{\omega}^{(1)} = \boldsymbol{\omega}^{(2)}\tan\delta$ according to the velocity relation at the contact point. The $\boldsymbol{\omega}^{(2)}$ and the velocity of the cutter along the tooth width direction $\mathbf{V}_{01}$ are collectively known as two degrees of freedom for meshing. These two parameters respectively control the coordinates of the tooth flanks in the tooth profile and tooth width direction.

2.2 Meshing equation of hypothetical plane gear and straight bevel gear

During the cutting process, the unit tangent vector is perpendicular to the relative velocity at the contact point between cutting surface and blank tooth surface [13]. In light of this, the relationship between relevant variables can be obtained by the following equation:

$$\mathbf{n}^{(1)} \cdot \mathbf{V}^{(12)} = 0 \tag{1}$$

where $\mathbf{n}^{(1)}$ is the unit tangent vector; $\mathbf{V}^{(12)}$ is the relative velocity. The two variables can be obtained as below.

In the initial position, coordinate system σ coincides with $\sigma^{(1)}$. Assuming that the coordinates of contact point M in σ are (x, y, z), the cutting face velocity of cutter $\mathbf{V}_1$ and the tooth surface velocity of the cutter $\mathbf{V}_2$ can be expressed as:

$$\mathbf{V}_1 = V_{01}\mathbf{i} - V_{02}\mathbf{k} \tag{2}$$

where $V_{02} = \omega_2 (R - L_1)\tan\delta$.

$$\mathbf{V}_2 = \boldsymbol{\omega}^{(2)} \times \mathbf{r}^{(2)} \tag{3}$$

where $\boldsymbol{\omega}^{(2)} = \omega_2 \mathbf{k}$; $\mathbf{r}^{(2)} = x\mathbf{i} + (y + (R - L_1)\tan\delta)\,\mathbf{j} + z\,\mathbf{k}$.

The relative velocity between the cutting surface and the tooth surface can be obtained by subtracting Eq. (3) from Eq. (2):

$$\mathbf{V}^{(12)} = y\omega_2\mathbf{i} - x\omega_2\mathbf{j} - V_{01}\mathbf{k} \tag{4}$$

Eq. (4) expresses the relative velocity $\mathbf{V}^{(12)}$ in σ at the initial position. For convenience, it is necessary to acquire the expression of relative velocity $\mathbf{V}^{(12)}$ in $\sigma^{(1)}$ at any meshing position. Thus, convert the radial vector $\mathbf{r}^{(1)}$ from $\sigma^{(1)}$ to σ, as shown in Eq. (5).

$$\mathbf{r} = \mathbf{M}_{01}\mathbf{r}^{(1)} + \mathbf{r}_{01} \tag{5}$$

where $\mathbf{r}^{(1)} = [x_1 y_1 z_1]^{\mathrm{T}}$; $\mathbf{M}_{01}$ is the coordinate transformation matrix of $\sigma^{(1)}$ to σ; $\mathbf{r}_{01}$ is the column matrix of origin O_1 in σ.

The relative velocity $\mathbf{V}^{(12)}$ in $\sigma^{(1)}$ can be determined by substituting the coordinates obtained in Eq. (5) to Eq. (4):

$$\mathbf{V}^{(12)} = y_1\omega_2\mathbf{i}_1 - (x_1 - \varphi_2(R - L_1)\tan\delta)\omega_2\mathbf{j}_1 - V_{01}\mathbf{k}_1 \tag{6}$$

where $\varphi_2 = \omega_2 t$.

The unit tangent vector $\mathbf{n}^{(1)}$ in Eq. (1) can be calculated by:

$$\mathbf{n}^{(1)} = \frac{\mathbf{r}_\mu^{(1)} \times \mathbf{r}_v^{(1)}}{\left|\mathbf{r}_\mu^{(1)} \times \mathbf{r}_v^{(1)}\right|} \tag{7}$$

where u and v are variables for cutting surface equations; $\mathbf{r}_\mu^{(1)}$ and $\mathbf{r}_v^{(1)}$ are the partial derivatives of u and v for cutting surface equations, respectively.

It can be seen that the solution to the meshing equation hinges on the accurate depiction of cutting surface equation.

3. CUTTING SURFACE EQUATION OF PLANNER

As shown in Fig. 2, the cutter has two cutting edges, each of which cuts one tooth surface of the gear. In each cutting edge, section *AD* handles the tooth surface, section *DE* processes the tooth root transition surface, and section *EF* treats the tooth root surface.

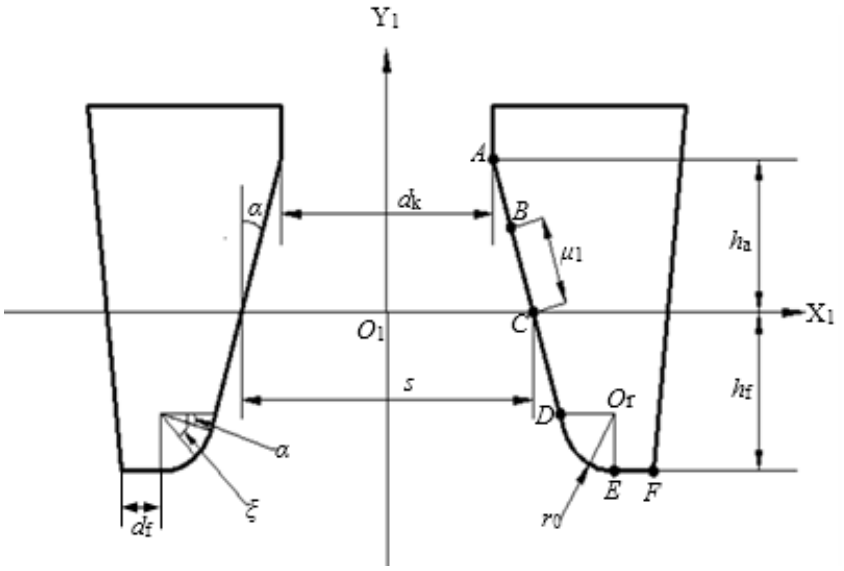

Figure 2: Cutter profile.

Note: α is the tooth profile angle; s equals the tooth thickness of the target gear; h_f is the dedendum; h_a is the addendum; d_k is the tooth top width; d_f is the half width of the tooth bottom of the target gear; r_0 is corner radius of the cutter; ξ is the angle between axis X_1 and the connecting line of a point on tool nose and circle centre; μ_1 is the distance between a point on segment AD and point C. The value of μ_1 is positive if point B is above axis X_1; otherwise, the value is negative. The length of segment CA is $\mu_a = h_a/cosa$, and that of segment CD is $\mu_f = (h_f - r_0 + r_0 \sin a)/cosa$.

The above parameters vary with the cross-section along the tooth width direction, which gradually narrows from the big end to the small end. The variation in key parameters can be expressed as:

$$h_a = h_{a1} - L_1 \tan\theta_a \tag{8}$$

where h_{a1} is big-end addendum of straight bevel gear.

$$h_f = h_{f1} - L_1 \tan\theta_f \tag{9}$$

where h_{f1} is big-end dedendum of straight bevel gear.

$$s = s_1(1 - \frac{L_1}{R}) \tag{10}$$

where s_1 is big-end tooth thickness of straight bevel gear.

The cutting surface equation of the cutter section can be obtained from the relationship between the parameters in Fig. 3.

Specifically, the cutting surface equation of segment AD can be expressed as:

$$\mathbf{r}^{(1)}(\mu_1, v) = (\frac{s}{2} - \mu_1 \sin\alpha)\mathbf{i}_1 + \mu_1 \cos\alpha \mathbf{j}_1 + v\mathbf{k}_1 \tag{11}$$

where $v \in [0, b]$ is the tooth width, with b being the cutter length; $\mu_1 \in (-\mu_f, \mu_a)$.

The cutting surface equation of segment DE can be expressed as:

$$\mathbf{r}^{(1)}(\xi, v) = (\frac{d}{2} - r_0 \cos\xi)\mathbf{i}_1 + (-h_f + r_0 \cos\xi)\mathbf{j}_1 + v\mathbf{k}_1 \tag{12}$$

where $d = s + 2(h_f - r_0)\tan\alpha + ((2r_0)/\cos\alpha)$; $\xi \in (0, \pi/2)$.

The cutting surface equation of segment EF can be expressed as:

$$\mathbf{r}^{(1)}\left(w,v\right) = w\mathbf{i}_1 - h_f\,\mathbf{j}_1 + v\mathbf{k}_1 \tag{13}$$

where $w \in (d/2, (d + d_f)/2)$.

Due to the symmetry of the cutter about the neutral axis, the author only gave the cutting surface equation on one side. The equation on the other side can be derived by symmetric transformation.

4. TOOTH SURFACE EQUATION

The tooth surface equations of straight bevel gear are essentially the coordinate transformation equation combined with the meshing equation.

$$\begin{cases} \mathbf{r}^{(2)} = \mathbf{M}_{21}\mathbf{r}^{(1)} + \mathbf{r}_{01}^{(2)} \\ \mathbf{r}_{01}^{(2)} = \mathbf{M}_{20}\mathbf{r}_{01} + \mathbf{r}_{0}^{(2)} \\ \mathbf{n}^{(1)} \cdot \mathbf{V}^{(12)} = 0 \end{cases} \tag{14}$$

where $\mathbf{r}^{(1)}$ corresponds to the Eqs. (12), (13), and (14) when solving the equations of tooth surface, tooth root transition surface and tooth surface, respectively; $\mathbf{M}_{20}$ and $\mathbf{M}_{21}$ are the coordinate transformation matrices of σ to $\sigma^{(2)}$ and $\sigma^{(1)}$ to $\sigma^{(2)}$, respectively; $\mathbf{r}_{01}^{(2)}$ and $\mathbf{r}_{0}^{(2)}$ are the column matrices of origin O_1 in $\sigma^{(2)}$ and origin O in $\sigma^{(2)}$, respectively.

The tooth surface equation in the Cartesian coordinate system can be obtained by substituting the cutting surface equation and the corresponding meshing equation into Eq. (14):

$$\begin{cases} x_2 = x_1\cos\varphi_2 - y_1\sin\varphi_2 + (R - L_1)\varphi_2\tan\alpha\cos\varphi_2 - (R - L_1)\tan\alpha\sin\varphi_2 \\ y_2 = x_1\sin\varphi_2 + y_1\cos\varphi_2 + (R - L_1)\varphi_2\tan\alpha\cos\varphi_2 + (R - L_1)\tan\alpha\sin\varphi_2 \\ z_2 = z_1 + L_1 \\ \mathbf{n}^{(1)} \cdot \mathbf{V}^{(12)} = 0 \end{cases} \tag{15}$$

where $z_2 \in [0, b_c]$, b_c is the tooth width of straight bevel gear; the fourth item corresponds to Eqs. (16), (17) and (18).

The bevel gear tooth surface obtained by the cutting movement of segment *AD* corresponds to the following meshing equation:

$$y_1\cos\alpha - (x_1 + (R - L_1)\varphi_2\tan\alpha)\sin\alpha = 0 \tag{16}$$

The bevel gear tooth root transition surface obtained by the cutting movement of segment *DE* corresponds to the following meshing equation:

$$y_1\sin\xi - (x_1 + (R - L_1)\varphi_2\tan\alpha)\cos\xi = 0 \tag{17}$$

The bevel gear tooth root surface obtained by the cutting movement of segment *EF* corresponds to the following meshing equation:

$$x_1 + (R - L_1)\varphi_2\tan\alpha = 0 \tag{18}$$

According to the meshing equation and cutting surface equation, the φ_2 is a function of the two independent variables μ_1 and L_1. In tooth surface equation, the two variables correspond to the two degrees of freedom in the principle of gear planning.

During the machining of a modified bevel gear, the cutter section was moved along axis Y_1 by a distance xm, where x is the modification coefficient and m is the cutter modulus. Then, the relevant parameters and tooth surface equation were calculated again.

5. PRECISE MODELLING AND SIMULATION ANALYSIS

5.1 Parametric modelling of straight bevel gear pair

According to the tooth surface equation obtained above, the parametric modelling of straight bevel gear pair was realized in software ANSYS. The tooth number, modulus, pressure angle and other basic parameters of the gear and the parameters of the cutter were inputted to create a gear model and a simplified finite-element assembly model. The modelling consists of the following steps in Fig. 3.

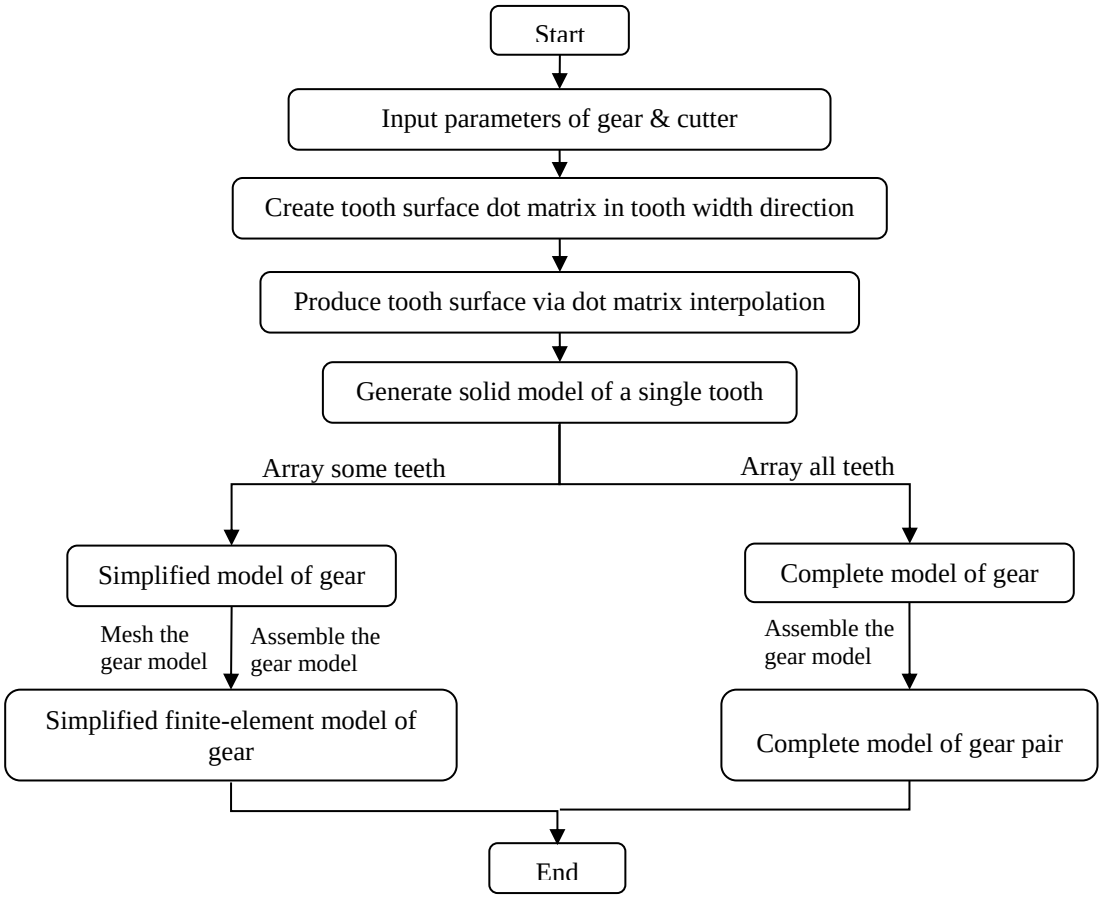

Figure 3: Workflow of parametric modelling of straight bevel gear.

To generate the tooth surface dot matrix, the tooth profile points were delaminated from the big end to the small end along the cutter movement path. Figure 4 shows the dot matrix of a single tooth surface.

To produce the simplified finite-element model for the simulation of straight bevel gear, the assembly model of five pairs of gear teeth was adopted to enhance analysis efficiency and accuracy, because at most two pairs of teeth are engaged during gear pair meshing. The third pair of gear teeth experienced the complete meshing process, and was thus selected as the research object. In the partial teeth finite-element model, the shaft hole was neglected as it has little impact on the meshing condition. The tooth surface and tooth root, as the targets of analysis, were meshed into much denser grids than the other parts.

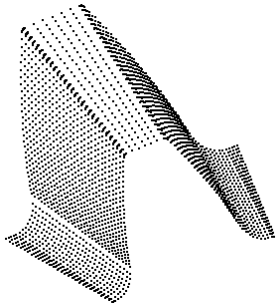

Figure 4: Dot matrix of a single tooth surface.

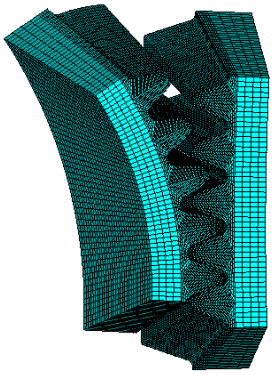

Figure 5: Simplified finite-element assembly model of straight bevel gear.

5.2 Meshing simulation analysis

The simulation analysis of straight bevel gear pair was conducted in ANSYS according to the transient meshing simulation method [14, 15]. The analysis focuses on tooth surface contact stress and tooth root bending stress, because the gear damages are mainly tooth pitting and fracture. As mentioned above, the third pair of teeth was taken as the object. Then, the stress-load curve of the object was drawn throughout the meshing process.

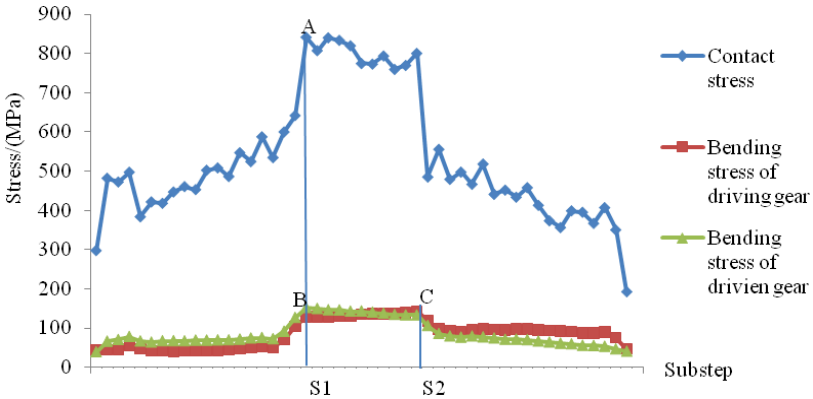

Figure 6: Stress-load curve of the third pair of teeth.

It can be seen from Fig. 6 that both contact stress and root bending stress underwent three phases, from the meshing of two teeth (two teeth meshing zone), the meshing of a single tooth (single tooth meshing zone), to the meshing of two teeth (two teeth meshing zone). The contact stress and the bending stress of the driven gear peaked simultaneously in step S1 [16], while the bending stress of the driving gear peaked in step S2.

The worst gear meshing position and the vulnerable positions of tooth surface and tooth root can be identified according to the load step information. Besides, the peak stresses can be used for strength analysis, laying the basis for optimizing the design of gear drive system.

6. SIMULATION EXAMPLE AND RESULT ANALYSIS

Based on the gear planning principle, this section develops a 3D model of straight bevel gear in the shape obtained by actual machining (the planning model). For comparison, other 3D models of straight bevel gear were created by traditional method (the traditional models), that is, ensuring that the tooth profile curve is spherical involute and replacing the tooth root transition curve with chamfer arc. To verify the feasibility and accuracy of our proposed modelling method, the author conducted repeated simulation experiments on the two types of models. One group of experiments were selected for detailed analysis. The basic parameters and working conditions are listed in Table I.

Table I: The basic parameters and working conditions of straight bevel gear.

Parameter	**Number of teeths** z	**Module** m	**Press angle** α (°)	**Modification coefficient** x	**Tooth width** B (mm)	**Input power** P (kw)	**Driving rotation speed** r (rpm)
Driving gear	19	3	20	0.41	24	9.8	1000
Driven gear	59	3	20	-0.41	24		

The type I cutter was selected in light of the data in Table I and the standard Straight Bevel Gear Generating Cutters (JIS B4351-2009) [17]. Then, the relevant cutter parameters were extracted, and the cutting surface equation was established. The parametric program of solid modelling and simulation analysis for bevel gear pair was achieved by the ANSYS APDL.

By the traditional method, the tooth surface was created by the spherical involute equation. The resultant surface was in line with the theoretical shape. However, a huge error occurred due to the replacement of the tooth root transition curve with the chamfer arc. There was no uniform standard for the radius of chamfer arc. Instead, the radius was placed roughly in the range of $0.2\,m$-$0.5\,m$.

Considering the chamfer arc differences of traditional models, three models with the chamfer arc radii of $0.28\,m$, $0.38\,m$ and $0.45\,m$ respectively were contrasted with the model created by our method.

6.1 Comparative analysis of tooth surface contact stress

As shown in Fig. 7, the third pair of teeth in the three traditional models experienced 51 load steps from engagement to disengagement. Among them, the load steps 21-32 fell in the single tooth meshing zone. By contrast, the third pair of teeth in the planning model underwent 50 load steps from engagement to disengagement, in which the load steps 21-31 belonged to the single tooth meshing zone.

Here, the gear tooth profile created by the gear planning principle based on hypothetical plane gear is called the planning tooth profile. If the cutting principle is based on a flat-top gear, the gear tooth profile will match the normal profile. The gear tooth profile created by the traditional method coincided with spherical involute, which is difficult to process. In general, the planning tooth profile was close to the spherical involute. Of course, it was more concave than the latter above the nodal point and more convex below the nodal point. The concave error was less than the convex error, both of which were controlled in the order of microns. The convex below the nodal point caused the third tooth of the driving gear to engage in advance. This is why the planning model has one fewer load step than the traditional model in single tooth meshing zone.

As can be seen from Fig. 7, the four models shared similar stress value and variation trend in the two teeth meshing zone (load steps 1-21). For the planning model, the contact stress

peaked (841.660 MPa) at the highest point of single tooth meshing zone of the driven gear; for traditional models, the contact stress peaked (793.777 MPa) at the highest point of single tooth meshing zone. In the subsequent two teeth meshing zone, the contact stress of planning model was lower than that of the three traditional models.

With relatively more teeth, the tooth profile of the driven gear teeth in the traditional models was rather straight, resulting in a small difference in tooth profile among the four driven gear models. The contact stress was mainly affected by the different shapes of the driving gear. After the 32nd load step, the spherical involute profile of the traditional models protruded more prominently above the nodal point than the planning profile of the planning model. Therefore, the teeth in the traditional models meshed more tightly with the driven gear tooth surface. This means the three traditional models had greater contact stress than the planning model in two teeth meshing zone. For the same reason, the contact stress of the traditional models peaked at the highest point of single tooth meshing zone of the driving gear rather than the driven gear.

In addition, the contact stress in single tooth meshing zone were on the rise, as the protrusion degree of tooth profile increased near the tooth root below the nodal point. When the three traditional models generated root chamfer arc surface, the local tooth profile changed inevitably, leading to the variation in contact stress.

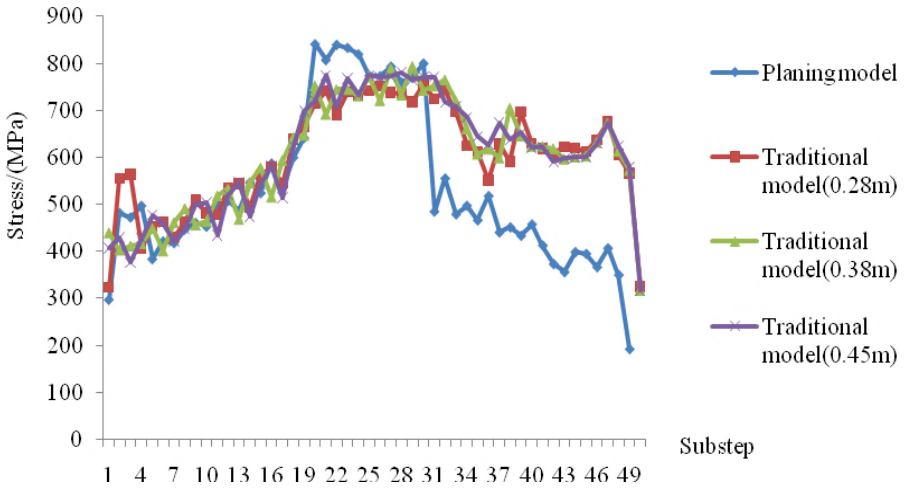

Figure 7: Contact stress of the third pair of teeth.

6.2 Comparative analysis of tooth root bending stress

The difference among the four models in tooth root transition surface was displayed intuitively by drawing the 3D models of the surface in CAD software.

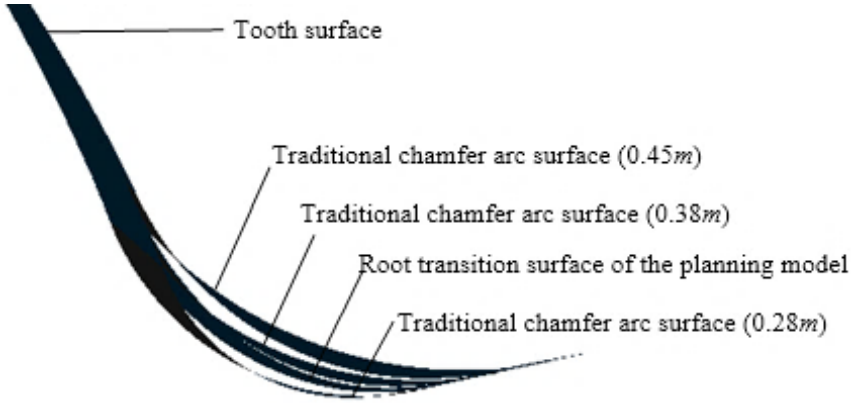

Figure 8: Comparison of four tooth root transition surfaces.

Fig. 8 reflects the shape error in traditional models arising from the different chamfer arc radii. Similarly, it is observed that the tooth root transition surface of the planning model differed significantly with the traditional chamfer arc surfaces. Furthermore, the shape error between tooth root transition surfaces was much greater than the error between tooth surfaces.

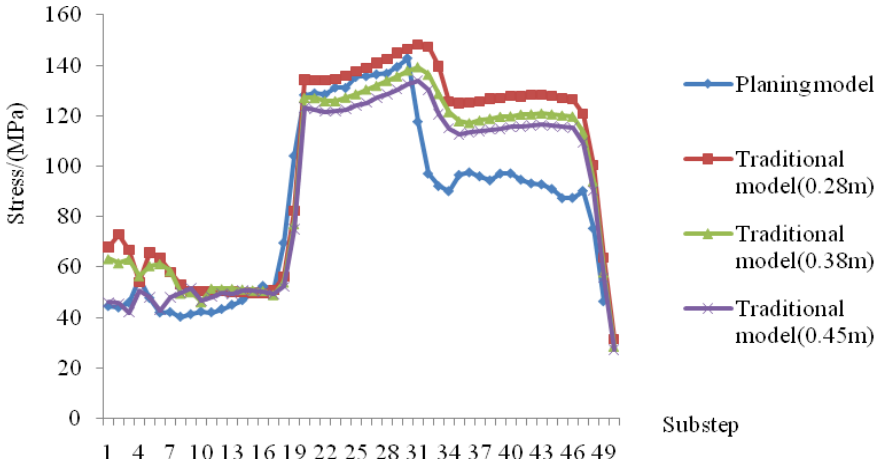

Figure 9: Driving gear bending stresses of the third pair of teeth.

As shown in Fig. 9, the driving gear bending stresses of all four models fluctuated at the beginning of the two teeth meshing zone (load steps 1-21). For the three traditional models, the tooth root bending stress of the driving gear decreased with the increase in the chamfer arc radius; for the planning model, the bending stress was lower than that of the traditional models, as its planning profile was slightly convex below the nodal point than the spherical involute.

After entering single tooth meshing zone, the 0.38 *m* radius model had a stress close to that of the planning model, because its chamfer arc surface was similar to the tooth root transition model of the latter. With the most protruding chamfer arc surface, the 0.45 *m* radius model had the smallest stress value. With the most recessed chamfer arc surface, the 0.28 *m* radius model had the greatest stress value.

In the subsequent two teeth meshing zone, the bending stress of the planning model was lower than that of the three traditional models. This is because a slight recess of planning profile above the nodal point brought about a smaller force arm, such that a partial load was shared by the tooth root profile of the next teeth. The maximum root bending stress of the driving gear in the planning model was 142.903 MPa, 2.58 % lower than that of the traditional models (146.595 MPa).

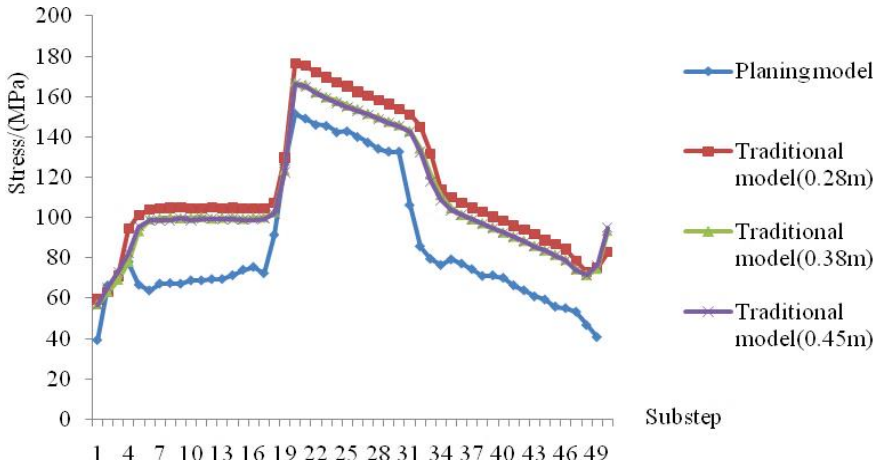

Figure 10: Driven gear bending stresses of the third pair of teeth.

As shown in Fig. 10, the driven gear bending stress of the planning model was below that of the three traditional models throughout the meshing process. This is attributable to the smaller force arm and thicker root resulted from the tooth profile shape difference between the planning model and the traditional models. The maximum root bending stress of the driven gear in the planning model was 151.476 MPa, 16.44 % lower than that of the traditional models (176.383 MPa).

7. CONCLUSION

Based on the gear planning principle, this paper deduces the equations for tooth surface, tooth root surface and tooth root transition surface of straight bevel gear. Then, the 3D assembly model of gear pair was established according to these equations, and the transient meshing simulation was performed on a simplified gear pair model. The model was contrasted with three traditional models to verify its feasibility. The further analysis of root bending stress illustrates superiority of the modelling method in strength analysis and optimization of gear structure. The following conclusions were drawn from the research.

(1) The tooth surface contact condition of straight bevel gear relies heavily on the modelling principle. Each modelling principle gives birth to a unique shape of tooth surface, which, in turn, determines the specific value and trend of tooth surface contact stress in the meshing process.

(2) The spherical involute profile of the traditional modelling method satisfies the meshing requirements of straight bevel gear. However, a huge error occurred in model shape and stress value due to the replacement of the tooth root transition curve with the chamfer arc, which drags down the economy and stability of the transmission design.

(3) The modelling method based on gear planning principle is more accurate than the traditional modelling method. By this method, the shape of both tooth surface and tooth root transition surface agrees well with the actual shape obtained by gear planning. Thus, this method sheds new light on the optimization of gear structure design and the economy of gear production.

Of course, the author did not elaborate on the optimization of straight bevel gear design with the proposed method and analysis results. This issue will be tackled in the next research.

ACKNOWLEDGEMENT

This work was supported by the National Natural Science Foundation of China (Grant No. 51674155), the Special Funds for Cultivation of Taishan Scholars and the Science and Technology Development Program of Shandong Province (Grant No. 2017GGX30127).

REFERENCES

[1] Bahramighahnavieh, A.; Mosaddegh, P.; Akbarzadeh, S. (2013). Investigation of the Hertzian stress distribution on the surface of the straight bevel gear, *Applied Mechanics and Materials*, Vol. 307, 304-307, doi:10.4028/www.scientific.net/AMM.307.304

[2] Zolfaghari, A.; Goharimanesh, M.; Akbari, A. A. (2017). Optimum design of straight bevel gears pair using evolutionary algorithms, *Journal of the Brazilian Society of Mechanical Sciences and Engineering*, Vol. 39, No. 6, 2121-2129, doi:10.1007/s40430-017-0733-9

[3] Zhang, F.-Y.; Tian, X.-J.; Cui, H.-Y. (2012). The modification design of involute straight bevel gear, *IERI Procedia*, Vol. 3, 52-59, doi:10.1016/j.ieri.2012.09.010

[4] Lou, J. J.; Cao, X. M.; Jiao, J. S. (2013).Tooth surface contact stress analysis of the straight bevel gear axial practice, *Applied Mechanics and Materials*, Vol. 401-403, 345-349, doi:10.4028/www.scientific.net/AMM.401-403.345

[5] Zhang, D.-Y.; Liu, S.-G.; Liu, B.-L.; Hong, J. (2013).Investigation on bending fatigue failure of a micro-gear through finite element analysis, *Engineering Failure Analysis*, Vol. 31, 225-235, doi:10.1016/j.engfailanal.2013.02.003

[6] Ozel, C.; Inan, A.; Ozler, L. (2005). An investigation on manufacturing of the straight bevel gear using end mill by CNC milling machine, *Journal of Manufacturing Science and Engineering*, Vol. 127, No. 3, 503-511, doi:10.1115/1.1863256

[7] Li, D. Q.; He, Y. M.; Deng, X. Z.; Zhang, L. X.; Zheng, X. L. (2013).Computerized generation simulation of straight bevel gears with tangear, *Advanced Materials Research*, Vol. 711, 318-322, doi:10.4028/www.scientific.net/AMR.711.318

[8] Shih, Y.-P.; Hsieh, H.-Y. (2015). Straight bevel gear generation using the dual interlocking circular cutter cutting method on a computer numerical control bevel gear-cutting machine, *Journal of Manufacturing Science and Engineering*, Vol. 138, No. 2, Paper 021007, 11 pages, doi:10.1115/1.4030937

[9] Fuentes, A.; Iserte, J. L.; Gonzalez-Perez, I.; Sanchez-Marin, F. T. (2011). Computerized design of advanced straight and skew bevel gears produced by precision forging, *Computer Methods in Applied Mechanics and Engineering*, Vol. 200, No. 29-32, 2363-2377, doi:10.1016/j.cma.2011.04.006

[10] Cui, D. L.; Li, Y. T.; Zhang, H. Z. (2012). Finite element analysis on bending stress of generating spur bevel gear based on ANSYS, *Advanced Materials Research*, Vol. 490-495, 2546-2549, doi:10.4028/www.scientific.net/AMR.490-495.2546

[11] Nalluveettil, S. J.; Muthuveerappan, G. (1993). Finite element modelling and analysis of a straight bevel gear tooth, *Computers & Structures*, Vol. 48, No. 4, 739-744, doi:10.1016/0045-7949(93)90268-I

[12] Deng, S.; Hua, L.; Han, X.-H.; Huang, S. (2013). Finite element analysis of contact fatigue and bending fatigue of a theoretical assembling straight bevel gear pair, *Journal of Central South University*, Vol. 20, No. 2, 279-292, doi:10.1007/s11771-013-1486-y

[13] Litvin, F. L.; Fuentes, A. (2004). *Gear Geometry and Applied Theory*, 2nd ed., Cambridge University Press, Cambridge

[14] Li, X. Y.; Wang, N. N.; Lv, Y. G.; Zeng, Q. L.; Hidenori, K. (2016). Tooth profile modification and simulation analysis of involute spur gear, *International Journal of Simulation Modelling*, Vol. 15, No. 4, 649-662, doi:10.2507/IJSIMM15(4)6.358

[15] Li, X. Y.; Zhang, Q. X.; Wang, N. N.; Zeng, Q. L.; Hidenori, K. (2017). Meshing simulation and strength calculation of a carburized gear pair, *International Journal of Simulation Modelling*, Vol. 16, No. 1, 121-132, doi:10.2507/IJSIMM16(1)10.376

[16] Zeng, Q. L.; Wang, K.; Wan, L. R.; Zhang, X. (2017). Accurate modelling and transient meshing analysis of involute spur gear based on the principle of gear shaping, *International Journal of Simulation Modelling*, Vol. 16, No. 2, 322-333, doi:10.2507/IJSIMM16(2)CO7

[17] JIS B-4351. (2013). *Straight Bevel Gear Generating Cutter (Type G)*, Japanese Standards Association, Tokyo